Toxicology and Applied Pharmacology 257 (2011) 388–395

Contents lists available at SciVerse ScienceDirect

Toxicology and Applied Pharmacology

journal homepage: www.elsevier.com/locate/ytaap

A superoxide anion-scavenger, 1,3-selenazolidin-4-one suppresses serum deprivation-induced apoptosis in PC12 cells by activating MAP kinase

Atsuyoshi Nishina [a,*], Hirokazu Kimura [b], Kunihisa Kozawa [b], Geoffroy Sommen [c], Takao Nakamura [d], Heinz Heimgartner [e], Mamoru Koketsu [f], Shoei Furukawa [g]

[a] Yonezawa Women's Junior College, 6-15-1 Tohrimachi, Yonezawa, Yamagata 992-0025, Japan
[b] Gunma Prefectural Institute of Public Health and Environmental Sciences, 378 Kamioki, Maebashi, Gunma 371-0052, Japan
[c] Lonza Braine SA, Chaussée de Tubize 297, B-1420 Braine l'Alleud, Belgium
[d] Department of Biomedical Information Engineering, Graduate School of Medical Science, Yamagata University, Yamagata 990-9585, Japan
[e] University of Zürich, Institut of Organic Chemistry, Winterthurerstrasse 190, CH-8057 Zürich, Switzerland
[f] Department of Materials Science and Technology, Faculty of Engineering, Gifu University, Gifu 501-1193, Japan
[g] Laboratory of Molecular Biology, Gifu Pharmaceutical University, 5-6-1 Mitahora-higashi, Gifu 502-8585, Japan

ARTICLE INFO

Article history:
Received 2 August 2011
Revised 20 September 2011
Accepted 23 September 2011
Available online 2 October 2011

Keywords:
Selenazolidine
Superoxide radicals
Scavenging effect
PC 12 sells
MAP kinase
Phosphorylation

ABSTRACT

Synthetic organic selenium compounds, such as ebselen, may show glutathione peroxidase-like antioxidant activity and have a neurotrophic effect. We synthesized 1,3-selenazolidin-4-ones, new types of synthetic organic selenium compounds (five-member ring compounds), to study their possible applications as antioxidants or neurotrophic-like molecules. Their superoxide radical scavenging effects were assessed using the quantitative, highly sensitive method of real-time kinetic chemiluminescence. At 166 μM, the O_2^- scavenging activity of 1,3-selenazolidin-4-ones ranged from 0 to 66.2%. 2-[3-(4-Methoxyphenyl)-4-oxo-1,3-selenazolidin-2-ylidene]malononitrile (compound **b**) showed the strongest superoxide anion-scavenging activity among the 6 kinds of 2-methylene-1,3-selenazolidin-4-ones examined. Compound **b** had a 50% inhibitory concentration (IC_{50}) at 92.4 μM and acted as an effective and potentially useful O_2^- scavenger *in vitro*. The effect of compound **b** on rat pheochromocytome cell line PC12 cells was compared with that of ebselen or nerve growth factor (NGF) by use of the MTT [3-(4, 5-dimethyl-2-thiazolyl)-2,5-diphenyl-2*H*-tetrazolium bromide] assay. When ebselen was added at 100 μM or more, toxicity toward PC12 cells was evident. On the contrary, compound **b** suppressed serum deprivation-induced apoptosis in PC12 cells more effectively at a concentration of 100 μM. The activity of compound **b** to phosphorylate mitogen-activated protein kinase/extracellular signal-regulated protein kinase (ERK) 1/2 (MAP kinase) in PC12 cells was higher than that of ebselen, and the former at 100 μM induced the phosphorylation of MAP kinase to a degree similar to that induced by NGF. From these results, we conclude that this superoxide anion-scavenger, compound **b**, suppressed serum deprivation-induced apoptosis by promoting the phosphorylation of MAP kinase.

Introduction

A relatively large amount of O_2^- is generated in mitochondria of the cardiovascular system, and in phagocytes including polymorphonuclear leukocytes (PMNs), macrophages/monocytes, eosinophils, mast cells, and basophils (Fridovich, 1983). O_2^- reacts not only with biomolecules, but also with other reactive oxygen species (ROS), such as hydrogen peroxide (H_2O_2) and lipid radicals (LOOH) (Balaban et al., 2005; Fridovich, 1998; Meydani et al., 1992). Additionally, ROS derived from leukocytes induce excessive inflammation, leading to cell/tissue injuries (Berridge, 1984; Curnutte et al., 1974). In extreme instances such as endotoxin shock, neutrophils kill the infected host (Ryter et al., 2007), and therefore the generation of ROS must be controlled (Long et al., 1997; Ramirez et al., 2003).

Superoxide dismutases (SODs), catalase, glutathione peroxidase (GPX), and some vitamins are representative antioxidants, and these molecules act as protectors against ROS-induced toxicity in cells (Fridovich, 1995; Kimura et al., 2005). GPX is believed to be an important antioxidant enzyme, and it effectively reduces the toxicity of H_2O_2 *in vitro* and *in vivo* (Kimura et al., 2005; Wendel and Tiegs, 1986). The active site of GPX contains selenium atoms (Wendel and Tiegs, 1986), and various studies have shown that selenoproteins, including GPX, reduce oxidative stress in cells (Jeong et al., 2002; Tiano et al., 2000). Thus, various organic selenium compounds may be potent candidate scavengers of ROS.

Ebselen®, a five-member ring selenium-containing heterocyclic compound showing GPX-like activity (Engman, 1989), is a typical synthetic antioxidant for the scavenging of ROS (Zhang et al., 2002).

* Corresponding author. Fax: +81 238 22 7333, +81 58 230 1893.
E-mail address: nishina@yone.ac.jp (A. Nishina).

0041-008X/$ – see front matter © 2011 Elsevier Inc. All rights reserved.
doi:10.1016/j.taap.2011.09.022

The antioxidative effects are due to selective blockade of leukocyte infiltration and activation, which results in elimination of these ROS (Zhang et al., 2002). Thus, ebselen is a multifunctional antioxidant having a potential chemopreventive effect on inflammation (Nakamura et al., 2002). On the basis of these facts, various types of organic selenium compounds might be applicable for the reduction of oxidative stresses (Takahashi et al., 2004, 2005a,b).

Morey et al. (2001) demonstrated that some selenoproteins, such as selenoprotein P, regulate the redox potential in cells, resulting in modulation of various phosphorylation pathways including Ras/MAP kinase signaling (Morey et al., 2001). On the other hand, we demonstrated earlier that ebselen regulates the redox in PC12 cells and induces activation of the MAP kinase cascade and neuronal differentiation *via* regulation of kinases or phosphatases related to intercellular signaling (Nishina et al., 2008). Thus, such selenium compounds may act not only as ROS scavengers, but also as intracellular signal regulators.

We have synthesized various organic selenium compounds, such as selenoamides (Takahashi et al., 2004), selenoureas, thioureas (Takahashi et al., 2005b), and selenocarbamates (Takahashi et al., 2005a), and found that most of these compounds act as effective scavengers of O_2^- *in vitro* (Takahashi et al., 2005a,b). In the present study, we newly synthesized five-member ring compounds, 1,3-selenazolidin-4-ones, and tested not only their superoxide radical-scavenging activity (SOSA) by using a real-time kinetic chemiluminescence method, but also their suppressive activity toward serum deprivation-induced apoptosis and their ability to induce MAP kinase phosphorylation in PC12 cells.

Materials and methods

Materials. 2-[3-(Aryl)-4-oxo-1,3-selenazolidin-2-ylidene] malononitriles (compound **b**) were prepared according to procedures previously reported (Sommen et al., 2006). A Cypridina luciferin analogue, 2-methyl-6-(4-methoxyphenyl)-3,7-dihydroimidazo-[1,2-]pyrazin-3-one hydrochloride (MCLA) was obtained from Tokyo Kasei (Tokyo, Japan) as a chemiluminescent probe for superoxide radicals. MCLA was dissolved in doubly distilled water and stored at −80 °C prior to usage. The concentration of the MCLA solution was determined based on its absorbance at 430 nm and an absorbance coefficient value of $\varepsilon = 9600\ M^{-1}\ cm^{-1}$, as previously described (Kimura and Nakano, 1988). SOD (lyophilized powder, 3400 units/mg protein) and xanthine oxidase (XOD grade III) were purchased from Sigma Chemical Co. (St. Louis, MO, USA). Hypoxanthine was obtained from Wako Pure Chemical Industries Ltd. (Osaka, Japan) and used without further purification. All other chemicals and solvents were analytical grade and used without further purification.

Methods for the synthesis of 2-[3-(aryl)-4-oxo-1,3-selenazolidin-2-ylidene]malononitriles (a–f). A 25-ml round-bottom flask equipped with a magnetic stirrer and condenser was charged with a solution of malononitrile (73 mg, 1.1 mmol) in DMF (10 ml). Triethylamine (0.15 ml, 1.1 mmol) was then added, and the mixture was stirred for 30 min at room temperature (RT). Next, the appropriate isoselenocyanate (1.1 mmol) was added and the mixture stirred for 1 h at RT. The halogenated compound (1.1 mmol) was then added dropwise, and the mixture was stirred for 4 h before being evaporated to dryness under reduced pressure. The crude product was purified by column chromatography on silica gel with hexane–ethyl acetate (100/0–50/50) as the eluant and recrystallized from ethyl acetate.

2-(4-Oxo-3-phenyl-1,3-selenazolidin-2-ylidene)-malononitrile, Compound **a**. Yield: 235–270 mg (74–85%). Colorless crystals. Mp 265–267 °C. IR: 2985w, 2216 s, 1733 s, 1596w, 1522 s, 1493 m, 1368 m, 1223 s, 851w, 758w, 698 m. ^{1}H-NMR (300 MHz, $CDCl_3$): δ 4.39 (s, CH_2), 7.43 (d-like, $J = 7.9$ Hz, 2 arom. H), 7.50–7.60 (m, 3 arom. H). ^{13}C-NMR (75 MHz, $CDCl_3$): δ 29.1, 56.7, 110.1, 115.1, 128.9, 129.4, 130.8, 134.8, 173.3, 173.9. CI-MS: 307 (100, $[M(^{80}Se) + NH_4]^+$); CI-MS (i-butane): 290 (100, $[M(^{80}Se) + 1]^+$). Anal. calcd for $C_{12}H_7N_3OSe$ (288.16): C 50.02, H 2.45, N 14.58; found: C 49.98, H 2.60, N 14.34.

2-[3-(4-Methoxyphenyl)-4-oxo-1,3-selenazolidin-2-ylidene]malononitrile, Compound **b**. Yield: 259 mg (74%). Orange crystals. Mp 193–195 °C. IR: 2945w, 2216 m, 2210 m, 1752 m, 1606w, 1523 s, 1508 s, 1369 m, 1303w, 1255 m, 1212 m, 1015w, 822w. ^{1}H-NMR (300 MHz, $CDCl_3$): δ 3.83 (s, CH_3O), 4.38 (s, CH_2), 7.07, 7.35 (AA′BB′, $J_{AB} = 8.0$ Hz, 4 arom. H). ^{13}C-NMR (75 MHz, $CDCl_3$): δ 28.9, 55.4), 56.6, 110.2, 114.6, 115.1, 127.3, 130.2, 132.4, 160.8, 173.9. CI-MS: 337 (100, $[M(^{80}Se) + NH_4]^+$). Anal. calcd for $C_{13}H_9N_3O_2Se$ (318.20): C 49.07, H 2.85, N 13.21; found: C 48.84, H 3.01, N 13.57.

2-[3-(2,6-Dimethylphenyl)-4-oxo-1,3-selenazolidin-2-ylidene]malononitrile, Compound **c**. Yield: 289 mg (83%). Colorless crystals. Mp 296–298 °C. IR: 3000w, 2944w, 2217 s, 2206 s, 1742 s, 1517 s, 1474 m, 1392w, 1352 s, 1217 m, 1205 s, 1183 m, 1151 m, 1035w, 837w, 785 m, 736w. ^{1}H-NMR (300 MHz, $CDCl_3$): δ 2.16 (s, $2CH_3$), 4.72 (s, CH_2), 7.28 (d, $J = 7.8$ Hz, 2 arom. H), 7.44 (t, $J = 7.9$ Hz, 1 arom. H). ^{13}C-NMR (75 MHz, $CDCl_3$): δ 16.7, 28.7, 57.1, 109.3, 114.7, 128.3, 130.9, 132.4, 136.5, 171.5, 173.3. CI-MS: 335 (100, $[M(^{80}Se) + NH_4]^+$). Anal. calcd for $C_{14}H_{11}N_3OSe$ (316.22): C 53.18, H 3.51, N 13.29; found: C 53.18, H 3.58, N 13.03.

2-[3-(4-Fluorophenyl)-4-oxo-1,3-selenazolidin-2-ylidene]malononitrile, Compound **d**. Yield: 280 mg (83%). Colorless crystals. Mp 244–246 °C. IR: 2995w, 2982w, 2219 s, 2210 s, 1737 s, 1600w, 1528 s, 1516 s, 1507 s, 1373 m, 1222 s, 1208 s, 1161w, 858w, 826w, 791w. ^{1}H-NMR (300 MHz, $CDCl_3$): δ 4.65 (s, CH_2), 7.67 (t-like, $J = 9.0$ Hz, 2 arom. H), 7.49–7.59 (m, 2 arom. H). ^{13}C-NMR (75 MHz, $CDCl_3$): δ 29.0, 56.7, 110.2, 114.9, 116.4 (d, $^2J_{CF} = 23$ Hz, 2CH), 131.1, 131.5 (d, $^3J_{CF} = 9$ Hz, 2CH), 163.2 (d, $^1J_{CF} = 248$ Hz, CF), 173.7, 173.9. CI-MS: 325 (100, $[M(^{80}Se) + NH_4]^+$). Anal. calcd for $C_{12}H_6N_3OSeF$ (306.16): C 47.08, H 1.98, N 13.73; found: C 47.01, H 2.21, N 14.02.

2-[3-(4-Chlorophenyl)-4-oxo-1,3-selenazolidin-2-ylidene]malononitrile, Compound **e**. Yield: 242 mg (68%). Colorless crystals. Mp 245–247 °C. IR: 2947w, 2223 m, 2213 m, 1733 s, 1529 s, 1485 m, 1404w, 1370 m, 1219 s, 1172w, 1084w, 1015w, 845w, 813w, 722w. ^{1}H-NMR (300 MHz, $CDCl_3$): δ 4.33 (s, CH_2), 7.45, 7.58 (AA′BB′, $J_{AB} = 8.7$ Hz, 4 arom. H). ^{13}C-NMR (75 MHz, $CDCl_3$): δ 29.1, 56.7, 110.3, 114.9, 129.5, 131.0, 133.7, 135.5, 173.4, 173.8. CI-MS: 341 (100, $[M(^{80}Se, ^{35}Cl) + NH_4]^+$). Anal. calcd for $C_{12}H_6N_3OSeCl$ (322.61): C 44.68, H 1.87, N 13.03; found: C 44.75, H 2.10, N 12.92.

2-[3-(4-Bromophenyl)-4-oxo-1,3-selenazolidin-2-ylidene]malononitrile, Compound **f**. Yield: 351–38 3 mg (87–95%). Colorless crystals. Mp 247–249 °C. IR: 2947w, 2222 s, 2211 s, 1736 s, 1585w, 1526 s, 1481 s, 1399w, 1371 m, 1218 s, 1171 m, 1066w, 1012 m, 842 m, 809 m, 711w. ^{1}H-NMR (300 MHz, $CDCl_3$): δ 4.67 (s, CH_2), 7.71, 8.05 (AA′BB′, $J_{AB} = 8.7$ Hz, 4 arom. H). ^{13}C-NMR (75 MHz, $CDCl_3$): δ 29.1, 56.8, 110.3, 114.9, 129.5, 131.0, 133.7, 135.6, 173.4, 173.8. CI-MS: 387 (79, $[M(^{80}Se, ^{81}Br) + NH_4]^+$), 385 (100, $[M(^{80}Se, ^{79}Br) + NH_4]^+$). Anal. calcd for $C_{12}H_6N_3OSeBr$ (367.07): C 39.27, H 1.65, N 11.45; found: C 39.44, H 1.86, N 11.49.

Assay of superoxide anion-scavenging activity (SOSA). SOSA of 2-[3-(aryl)-4-oxo-1,3-selenazolidin-2-ylidene]malononitriles (a–f) was measured by using a previously reported method (Kimura and Nakano, 1988). Briefly, the reaction mixture contained 5.8×10^{-7} M MCLA, 5×10^{-5} M hypoxanthine, xanthine oxidase (6.5 U), and 50 mM Tris–HCl buffer containing 0.1 mM EDTA at pH 7.8, in the presence or absence of various concentrations of compounds (a–f). To evaluate certain SOSA, we added SOD standard solutions (0.6–30 ng/ml) to the reaction mixture instead of compounds (a–f). The total volume was 3.0 ml. Compounds (a–f) (25 mM) were dissolved in dimethyl sulfoxide and stored at −80 °C prior to use. Chemiluminescence was measured by using a luminometer (Aloka, BLR201) at 25 °C. The reaction was initiated by the addition of MCLA to the standard incubation mixture excluding XOD, continued for 3 min without

XOD, and then for an additional 2 min after the addition of XOD. A representative example of a measurement showing the effect of compound **b** on MCLA-dependent luminescence is shown in Fig. 2. As compound **b** showed strong SOSA at 166 μM, we also measured the activity at 16.6, 41.5, and 83.0 μM. The percent inhibition of MCLA-dependent chemiluminescence was calculated as previously described (Kimura and Nakano, 1988). The 50% inhibitory concentration (IC_{50}) was calculated from 4 concentrations of compound **b** (16.6, 41.5, 83.0, and 166 μM). In this study, SOSA was measured twice for each sample and the mean value was used.

Cell culture. PC12 cells were cultured as described previously (Nishina et al., 2008). In brief, the cells were maintained in Dulbecco's modified Eagle's medium (DMEM; Sigma, St. Louis, MO) supplemented with 10% heat-inactivated horse serum (Gibco BRL, Grand Island, NY) and 5% heat-inactivated fetal bovine serum (FBS; Sanko Junyaku, Co., Ltd., Tokyo, Japan) or in serum-free medium [DMEM supplemented with 1% bovine serum albumin (BSA)], unless otherwise stated.

Calculation of cell numbers by MTT method. We serially prepared the cell suspensions (10^2 to 10^6 cells/ml) in DMEM supplemented with 10% FBS. Cell number was determined using a hemocytometer and cell viability always exceeded 98%, as determined by trypan blue exclusion. One hundred microliters of each cell suspension ($10–10^5$ cells/100 μl) was added to collagen-coated 96-well plates (Corning Incorporated Life Sciences, Lowell, MA) and incubated for 4 h at 37 °C in an atmosphere of 95% air/5% CO_2. After the incubation, 50 μg of MTT [3-(4,5-dimethyl-2-thiazolyl)-2,5-diphenyl-2*H*-tetrazolium bromide] was added to each well and incubated for 2 h at 37 °C in an atmosphere of 95% air/5% CO_2. Then, 50 μl of 50% (v/v) dimethyl formamide (DMFA) containing 20% (w/v) SDS was added to each well. Absorbance at 562 nm of the cell lysate in each well was directly measured using a microplate reader (Ultrospec Visible Plate Reader II, Amersham Biosciences, Tokyo, Japan). The calculation formula for determining the cell number was as follows: $Absorbance_{562\ nm} = 0.228e^{x/10,000,000}$ (e, natural logarithm; x, cell number). Using the method, we established a standard curve for each assay.

Measurement of cell viability and inhibition of caspase-3 and 7 activities. PC12 cells were seeded at a cell density of 2×10^6 cells/well into collagen-coated 96-well plates (Corning), and precultured in the above serum-containing medium for 2 days at 37 °C in an atmosphere of 95% air/5% CO_2. The cells were then cultured with DMEM containing 1% BSA and a given reagent for various numbers of days. The number of viable cells was evaluated by the above-mentioned method. Activities of caspase-3 and 7 were measured by the Caspase-Glo® 3/7 assay kit (Promega, Madison, WI) using Typhoon 9200 (Amersham Biosciences, Tokyo, Japan) in chemiluminescence mode.

Treatment with MAP kinase kinase (MEK1/2) inhibitor. Cells were preincubated with serum-free medium (DMEM supplemented with 1% BSA) containing 10 μM of U0126 (a MEK1/2 inhibitor) for 15 min, and transferred to and cultured in the serum-free medium supplemented with compound **b** or NGF for the appropriate periods of time. The effect of U0126 on the cell number was evaluated using the MTT assay, and that on morphology was evaluated by optical observation. Photographs were taken under phase-contrast observation at magnification 100×.

Detection of phosphorylated proteins. PC12 cells were cultured in serum-free medium containing a given test compound similarly as described in the previous section. Then the culture plates were placed on ice, and each well was washed with 3 ml of 2 mM Tris–HCl buffer, pH 8.0, (TBS) containing 0.33 M NaF and 6.25 M Na_3VO_4. The cells were subsequently lysed with 150 μl of 20 mM TBS containing 150 mM NaCl, 2 mM EDTA, 1% Nonidet P-40 (w/v), 1% sodium deoxycholate (w/v), 0.1% sodium dodecyl sulfate (SDS) (w/v), 50 mM NaF, 0.1% aprotinin (w/v), 0.1% leupeptin (w/v), 1 mM Na_3VO_4, and 1 mM phenylmethylsulfonyl fluoride. Cell lysates were collected using a cell scraper, transferred to 1.5 ml microcentrifuge tubes, and centrifuged at 15,000 ×g for 30 min at 4 °C. The supernatant was collected and transferred to another tube, and the overall protein concentration was determined using a BCA Protein Assay Reagent Kit (Pierce, Rockford, IL) with BSA as the standard.

Each supernatant containing proteins (20 μg aliquot) was mixed with sample buffer containing 4% SDS for SDS gel electrophoresis (SDS-PAGE) and incubated for 5 min at 80 °C. The protein samples were then subjected to the SDS-PAGE, and the proteins in gel were electroblotted onto polyvinylidene difluoride filters (Fluorotrans membrane W, 0.2 μm; Nihon Genetics, Tokyo, Japan). MAP kinase and its phosphorylated form were visualized by immunoblotting using monoclonal antibodies against p44/42 ERK and phospho p44/42 ERK, respectively (Cell Signaling Technology, Lake Placid, NY). Neurofilament M was similarly reacted with its primary antibody (Sigma). The membranes were then reacted with horseradish peroxidase-conjugated anti-rabbit or anti-mouse IgG antibody (Promega) as the secondary antibody. The blots were developed by the enhanced chemiluminescence method (Hyperfilm-ECL plus, Amersham Biosciences Corp., Piscataway, NJ).

Statistical analysis. The results are expressed as means ± SD. Significant difference from the control value was determined by using analysis of variance (ANOVA), followed by Dunnett's test. In all tests, statistical significance was set as *, $p<0.05$; **, $p<0.01$; ***, $p<0.005$.

Results

Superoxide radical-scavenging activity (SOSA) of 1,3-selenazolidin-4-one

The structures of 2-[3-(aryl)-4-oxo-1,3-selenazolidin-2-ylidene] malononitriles (compounds **a–f**) are shown in Fig. 1. Among them, only 2-[3-(4-methoxyphenyl)-4-oxo-1,3-selenazolidin-2-ylidene]malononitrile, compound **b**, had SOSA at 166 μM (66.2%). The other compounds, **a** and **c–f**, showed no activity. SOSA of compound **b** was dose-dependent (Fig. 2A). Compound **b** was sufficiently active to justify further testing after serial dilutions, and the IC_{50} was determined to be 92.4 μM (Fig. 2B). To determine whether compound **b** could eliminate superoxide anions generated by XOD, the amount of uric acid, the by-product of the superoxide anion in the standard reaction mixture, was measured with or without compound **b** (Fig. 3). Generation of uric acid was not significantly affected by adding a relatively high concentration of compound **b** (166 μM), suggesting that this compound **b** acts not as an inhibitor of XOD but as a scavenger of superoxide anions. On the other hand, SOSA at 166 μM of ebselen was 100%, and IC_{50} of ebselen was 20 μM.

Effect of compound b on PC12 cells in serum-deprived culture medium

In order to evaluate the effect of compound **b** or ebselen on PC12 cells in serum-deprived culture medium, we evaluated cell viability and caspase-3 and 7 activities by using the MTT assay and Caspase-Glo® 3/7 assay kit, respectively. Ebselen supplemented in the medium at 100 μM or higher showed toxic effects on the cells (Fig. 4A). On the other hand, cell viability was promoted by the addition of compound **b** or NGF (Figs. 4B, D). Compound **b** showed the maximum effect at 100 μM. Serum-deprived PC12 cells undergo apoptosis (Nishina et al., 2008), but the addition of NGF protects against this form of cell death (Biswas and Greene, 2002). Our present results thus suggest that compound **b** attenuated serum deprivation-induced apoptosis of PC12 cells.

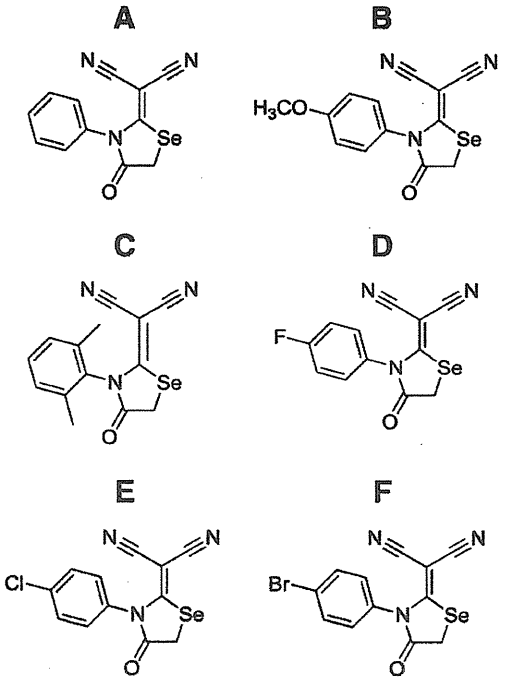

Fig. 1. 2-Methylene-1,3-selenaolidin-4-one derivatives tested in this study.

Furthermore, serum deprivation-induced activation of caspase-3 and 7 was also attenuated by the addition of compound **b** at 100 μM or higher; however, neither NGF nor ebselen showed such effect (Fig. 5).

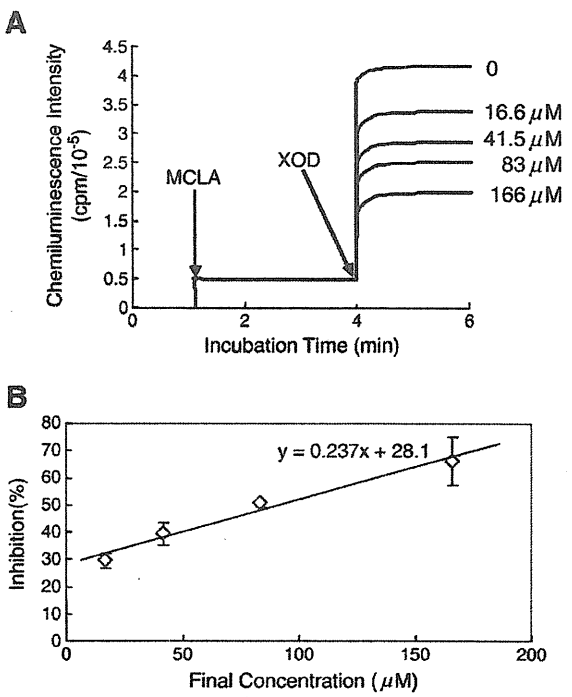

Fig. 2. Effect of 2-[3-(4-methoxyphenyl)-4-oxo-1,3-selenazolidin-2-ylidene]malononitrile, compound **b**, on (2-methyl-6-(4-methoxyphenyl)-3,7-dihydroimidazo-[1,2-a] pyrazin-3-one hydrochloride) (MCLA)-dependent luminescence. A: Chemiluminescence inhibition curves of compound **b**. Arrows indicate the times at which MCLA or xanthine oxidase (XOD) was added. B: Fifty-percent inhibitory concentration (IC_{50}) of the compound.

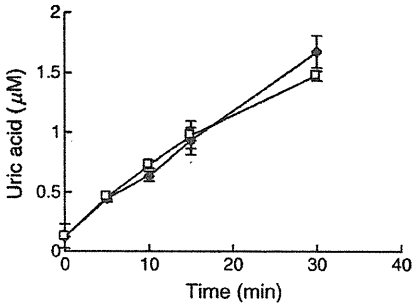

Fig. 3. Uric acid generation in a hypoxanthine–xanthine oxidase system. 2-[3-(4-Methoxyphenyl)-4-oxo-1,3-selenazolidin-2-ylidene]malononitrile **b** (166 μM) was added to the standard reaction mixture, and the rate of generation of uric acid was measured by using a uric acid measurement kit (L type WAKO UA M; Wako Pure Chemical Industries, Ltd. Osaka, Japan). The data are representative of 3 separate experiments and presented as the means ± SE. (-●-: Control, -□-: with **b**).

Effects of compound **b** *and U0126 on MAP kinase cascade and morphological changes in PC12 cells*

As it is reported that activation of the MAP kinase cascade represses apoptosis (Wang et al., 2008), the effect of U0126 (a MEK1/2 inhibitor) on the compound **b**- or NGF-facilitated cell viability was examined. The treatment with U0126 diminished the activity of compound **b** and NGF (Figs. 4C, D). Next, to clarify a relationship between cell viability and MAP kinase activation, we evaluated the effects of compound **b** and NGF on ERK1/2 phosphorylation. Compound **b** and NGF markedly stimulated ERK1/2 phosphorylation at 100 μM and 10 ng/ml, respectively, and the phosphorylation evoked by both compound **b** and NGF was significantly inhibited by the treatment with a MEK inhibitor, U0126 (Fig. 6), demonstrating that compound **b** stimulates ERK1/2 phosphorylation *via* MEK activation as well as NGF. ERK1/2 was significantly activated by the addition of 100 μM of compound **b**, but activation was low with 100 μM of ebselen.

The morphological changes in serum-deprived PC12 cells after treatment with compound **b**, NGF, and U0126 alone or in combination are shown in Fig. 7. After serum-deprivation, the cells with nuclear fragmentation increased in number with the increase of culture period, and the number of cells with normal morphology was severely decreased by 6 days (Fig. 7A). U0126 alone did not affect the cell morphology (Fig. 7B). NGF induced neurite outgrowth, and suppressed cell growth and nuclear fragmentation (Fig. 7C), but U0126 treatment completely suppressed these NGF-induced effects (Fig. 7D). Compound **b** stimulated the proliferation of PC12 cells and suppressed nuclear fragmentation, but U0126 treatment suppressed this effect. No morphological change was seen following the addition of 100 μM of ebselen (data not shown).

Discussion

We newly synthesized 6 organo-selenocompounds (Fig. 1), and as a result of comparing SOSA for each, we clarified that only 2-[3-(4-methoxyphenyl)-4-oxo-1,3-selenazolidin-2-ylidene]malononitrile (compound **b**) exhibited SOSA. Furthermore, the inhibition of serum deprivation-induced apoptosis of PC12 cells by compound **b** was observed.

Among the 6 compounds synthesized, only compound **b** had significant SOSA. As a possible reason for the mechanism, compound **b** bears a methoxy group at the para position of the benzene ring. The existence of an electron-donating group at this position of the benzene ring might contribute to SOSA. Previously, we systematically synthesized various organic selenium compounds, including selenocarbamates, selenoureas, thioureas, tertiary selenoamide compounds, 2-amino-1,3-selenazoles, and bis-(2-amino-5-selenazoyl) ketones,

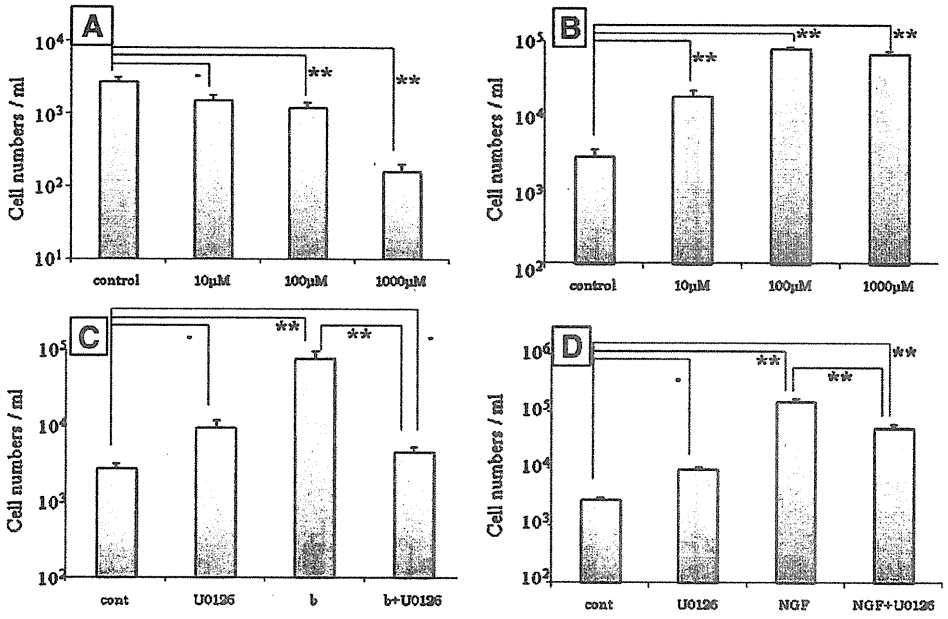

Fig. 4. Effects of ebselen, compound **b** or NGF on serum deprivation-induced apoptosis in PC12 cells. PC12 cells were cultured in serum-containing medium for 2 days. The cells were then preincubated with U0126 for 15 min (C, D) or not (A, B). Thereafter, the medium was changed to serum-free medium containing ebselen (A), compound **b** (B), compound **b** at 100 μM (C), NGF (D) or no reagents (*control*); and the cells were cultured for another 11 days. Data are expressed as mean ± SE. Significant differences of the values from the value of the control or no inhibitor at four days after serum deprivation were determined by ANOVA, followed by Dunnett's test. Significance: **, $p<0.01$; -, no significant difference.

and demonstrated their SOSA by using the same chemiluminescence method. The IC_{50} values of these compounds ranged from approximately 0.1 to 100 μM (Sekiguchi et al., 2005; Sekiguchi et al., 2006; Takahashi et al., 2004, 2005a,b). The SOSA of compound **b** might be relatively low compared with that of other compounds such as selenocarbamates, selenoureas, thioureas, tertiary selenoamide, and ebselen. On the other hand, compound **b** significantly inhibited serum deprivation-induced apoptosis in PC12 cells.

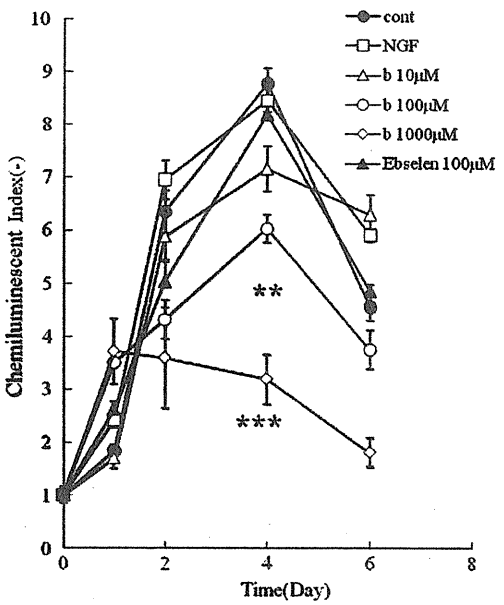

Fig. 5. Effects of compound **b**, NGF or ebselen on caspase-3 and -7 activation. PC12 cells were cultured in serum-containing medium for 2 days. Thereafter, the medium was changed to serum-free medium containing NGF, compound **b**, ebselen or no reagents (*control*); and the cells were cultured for another 6 days. Data are expressed as mean ± SE. Significant differences of the values from the value of the control at four days after serum deprivation were determined by ANOVA. Significance: ***, $p<0.005$; **, $p<0.01$.

U0126 significantly suppressed compound **b**-facilitated cell survival (Fig. 4C) and ERK1/2 phosphorylation (Fig. 6), suggesting that compound **b** promoted cell survival by the MEK-mediated activation of the MAP kinase pathway. On the other hand, serum deprivation-induced caspase-3 and 7 activation was attenuated by the addition of compound **b** in a concentration-dependent manner. Among 11 caspases so far identified, there are two types of apoptotic caspases: initiator (apical) caspases and effector (executioner) caspases. Initiator caspases (*e.g.* caspase-2, 8, 9 and 10) cleave inactive pro-forms of effector caspases, thereby activating them. Effector caspases (*e.g.* caspase-3, 6, and 7) in turn cleave other protein substrates within the cell, to trigger the apoptotic process (Sairanen et al., 2009). From the present results shown in Figs. 5 and 6, MAP kinase activation and suppression of the effector caspases were induced by compound **b** simultaneously. Thus, the inhibition of apoptosis in PC12 cells could be caused by both MAP kinase activation and effector caspase suppression by compound **b**. Because the activation of caspase-3 and 7 was not suppressed by NGF, apoptosis-inhibitory mechanisms of compound **b** were thought to be different from those of NGF.

At 1 mM of compound **b**, although the activities of caspase-3 and 7 were decreased, cell viability was attenuated compared with 100 μM of compound **b**. It is suggested that apoptosis in the PC12 cells is associated with not only these caspase activities but also activation or inactivation of another factor such as one from the Bcl family (Rong et al., 1999). In the present study, since only caspases and ERK1/2 were used as the index, no significant correlations were seen between concentration and effects. Further studies may be needed to confirm the role of the Bcl family in the compound **b**-affected PC12 cells, because relationship between concentration and activity of compound **b** is contradictory.

U0126 suppressed NGF-induced ERK1/2 phosphorylation and neurite outgrowth (Figs. 4D, 6 and 7D), but not cell survival. These observations were in good agreement with previous reports showing that the phosphorylation of ERK1/2 is necessary for neurite outgrowth from PC12 cells (Williams et al., 2000), and the activation of phosphoinositide 3-kinase for cell survival (Wert and Palfrey, 2000).

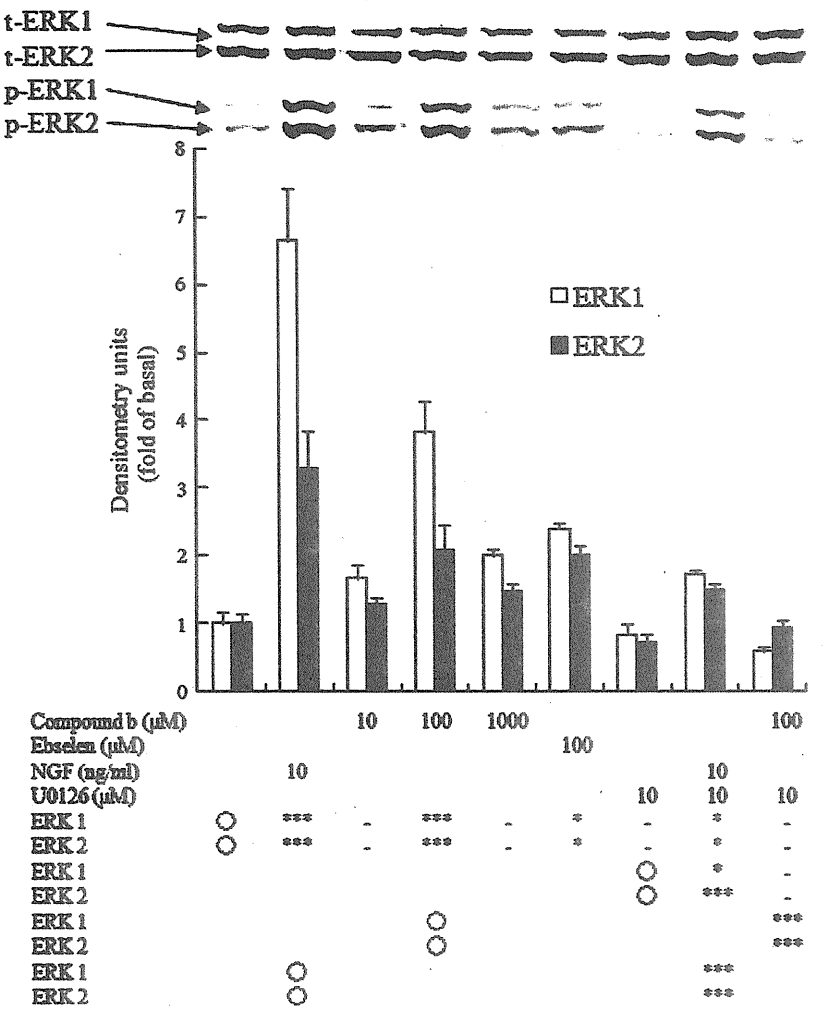

Fig. 6. Effects of compound **b**, NGF and/or U0126 on ERK1/2 activation. PC12 cells were cultured in serum-containing medium for 2 days. They were then preincubated with U0126 for 15 min or not, and thereafter treated or not with compound **b**, NGF or ebselen for 10 min. The phosphorylation of ERK1/2 of each sample was evaluated by immunoblotting. The intensity of each band of ERK1/2 was measured densitometrically, and the values are expressed as the mean ± SEM of fold-increase over the control value (treatment without any reagent) of 3 separate experiments. Significant differences of the values from the value of the corresponding control group were determined by ANOVA, followed by Dunnett's test. Control group was set as O. Significance: *, $P<0.05$; ***, $P<0.005$; -, no significant difference.

Previous reports suggested that sustained activation of ERK1/2 by Crk, and Shp-2 promotes the NGF-induced differentiation of PC12 cells (Matsuda et al., 1994; Wright et al., 1997). In other words, sustained ERK1/2 activation requires activation of Crk and Shp-2. In the present study, because the activation of ERK1/2 due to compound **b** may be transient, compound **b** only led to the inhibition of cell death (Aletta, 1994). Another report has suggested that the activation of caspases is associated with cell differentiation in PC12 cells (Vaisid et al., 2005). However, caspase-3 and 7 activities were not inhibited in the NGF-affected cells. Hence, further studies are needed to elucidate the precise mechanism involved in the differentiation of PC 12 cells and the relationship with caspase activities.

Ebselen, a well-known antioxidant containing a selenium atom in its molecule, was used for comparison with compound **b**. Unlike compound **b**, ebselen enhanced serum-deprived cell death at concentrations above 10 μM (Fig. 4A). Ebselen is a candidate therapeutic drug, and the toxicity of compound **b** was found to be lower than that of ebselen. Also, the effects of ebselen on the activation of ERK1/2 and the inactivation of caspases were lower than those of compound **b**. Therefore, in regard to the low toxicity and inhibition of apoptosis, compound **b** might be a more attractive and promising candidate than ebselen.

A low concentration of O_2^- produced in the human body generally plays a beneficial role in biological defenses and intercellular signal transduction (Kimura et al., 2005). Conversely, excessive O_2^- production has a role in the pathogenesis of many disorders, including inflammation, rheumatoid arthritis, and asthma (Kato et al., 2005; Vignola et al., 1998). Oxidative stress may be defined as an imbalance between cellular production of ROS and antioxidant defense mechanisms (Kimura et al., 2005), and ROS is a key component of inflammation and inflammatory disorders. The processes associated with inflammatory responses are complex and often involve ROS, including O_2^-. In this study, we demonstrated that our compounds functioned effectively as O_2^- scavengers *in vitro*, which action suggests that they suppress ROS overproduction through the elimination of excess O_2^-.

Intracellular signaling pathways involving enzyme activities of kinases and phosphatases are regulated by the redox state (Kamata et al., 2005). It is thought that there are two kinds of mechanisms involved in the compound **b**-induced ERK1/2 phosphorylation. One is the activation of cell membrane receptors and the other is regulation of the redox state in cells. Full disclosure of the effects of compound **b** on neuronal cells and the mechanism by which it activates ERK1/2 are expected to be reported in the near future. Although in this study only

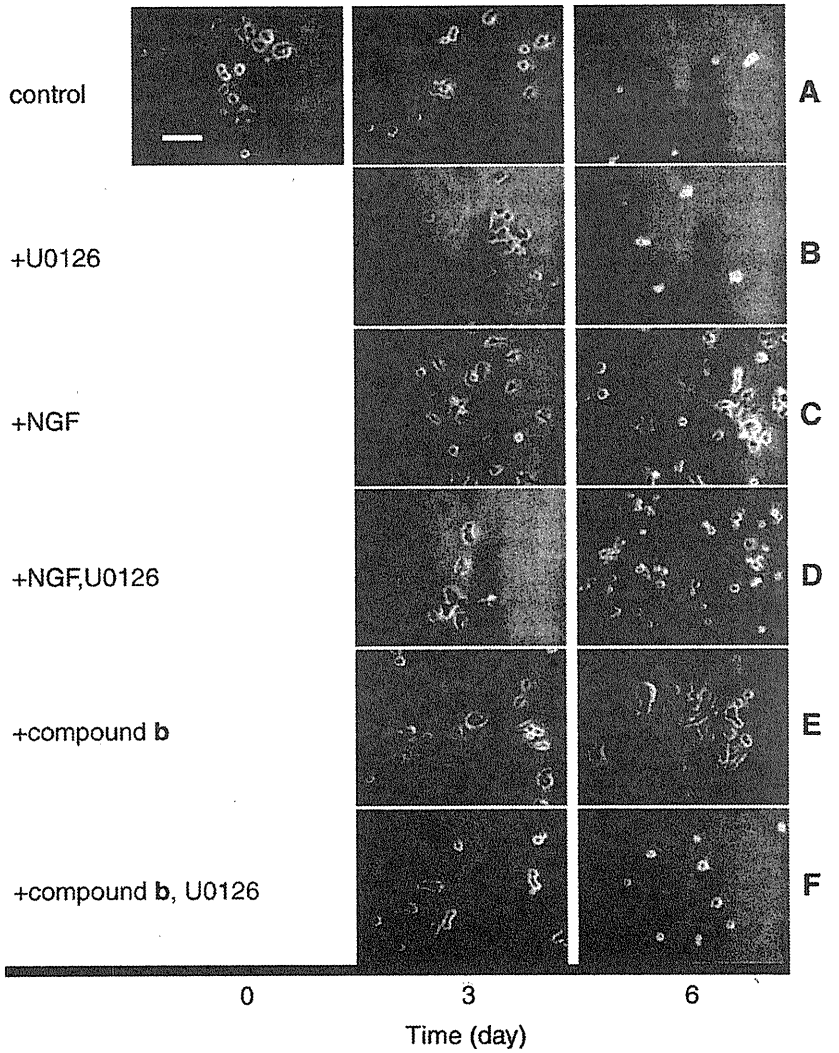

Fig. 7. Effect of U0126, compound **b** or NGF alone on cell survival of serum-deprived PC12 cells, and that of U0126 on NGF- or compound **b** promoted cell survival. PC12 cells were cultured in serum-containing medium for 2 days. The cells were preincubated with U0126 for 15 min (B, D, F) or not (A, C, E), and subsequently cultured for another 6 days in the serum-free medium supplemented with no reagents (A, B), NGF (10 ng/ml, C, D) or compound **b**(100 μM, E, F). Photographs were taken under phase-contrast observation at magnification 100×. Bar indicates 10 μm.

PC12 cells were used for biological evaluation of compound **b**, additional *in vitro* and *in vivo* studies are necessary to clarify whether this compound may be applicable as an antioxidant drug.

Conflict of interest statement

The authors declare that there are no conflicts of interest.

References

Aletta, J.M., 1994. Differential effect of NGF and EGF on ERK in neuronally differentiated PC12 cells. Neuroreport 5, 2090–2092.
Balaban, R.S., Nemoto, S., Finkel, T., 2005. Mitochondria, oxidants, and aging. Cell 120, 483–495.
Berridge, M.J., 1984. Inositol trisphosphate and diacylglycerol as second messengers. Biochem. J. 220, 345–360.
Biswas, S.C., Greene, L.A., 2002. Nerve growth factor (NGF) down-regulates the Bcl-2 homology 3 (BH3) domain-only protein Bim and suppresses its proapoptotic activity by phosphorylation. J. Biol. Chem. 277, 49511–49516.
Curnutte, J.T., Whitten, D.M., Babior, B.M., 1974. Defective superoxide production by granulocytes from patients with chronic granulomatous disease. N. Engl. J. Med. 290, 593–597.
Engman, L., 1989. Expedient synthesis of ebselen and related compounds. J. Org. Chem. 54, 2964–2966.
Fridovich, I., 1983. Superoxide radical: an endogenous toxicant. Annu. Rev. Pharmacol. Toxicol. 23, 239–257.
Fridovich, I., 1995. Superoxide radical and superoxide dismutases. Annu. Rev. Biochem. 64, 97–112.
Fridovich, I., 1998. Oxygen toxicity: a radical explanation. J. Exp. Biol. 201, 1203–1209.
Jeong, D.W., Kim, T.S., Chung, Y.W., Kim, I.Y., 2002. Selenoprotein W is a glutathione-dependent antioxidant *in vivo*. FEBS Lett. 517, 225–228.
Kamata, H., Oka, S., Shibukawa, Y., Kakuta, J., Hirata, H., 2005. Redox regulation of nerve growth factor-induced neuronal differentiation of PC12 cells through modulation of the nerve growth factor receptor, TrkA. Arch. Biochem. Biophys. 434, 16–25.
Kato, M., Hayashi, Y., Kimura, H., 2005. Oxygen radicals in inflammation and allergy related to viral infections. Curr. Drug Targets Inflamm. Allergy 4, 497–501.
Kimura, H., Nakano, M., 1988. Highly sensitive and reliable chemiluminescence method for the assay of superoxide dismutase in human erythrocytes. FEBS Lett. 239, 347–350.
Kimura, H., Sawada, T., Oshima, S., Kozawa, K., Ishioka, T., Kato, M., 2005. Toxicity and roles of reactive oxygen species. Curr. Drug Targets Inflamm. Allergy 4, 489–495.
Long, J.F., Dutta, P.K., Hogg, B.D., 1997. Fluorescence imaging of reactive oxygen metabolites generated in single macrophage cells (NR8383) upon phagocytosis of natural zeolite (erionite) fibers. Environ. Health Perspect. 105, 706–711.
Matsuda, M., Hashimoto, Y., Muroya, K., Hasegawa, H., Kurata, T., Tanaka, S., Nakamura, S., Hattori, S., 1994. CRK protein binds to two guanine nucleotide-releasing proteins for the Ras family and modulates nerve growth factor-induced activation of Ras in PC12 cells. Mol. Cell. Biol. 14, 5495–5500.
Meydani, M., Evans, W., Handelman, G., Fielding, R.A., Meydani, S.N., Fiatarone, M.A., Blumberg, J.B., Cannon, J.G., 1992. Antioxidant response to exercise-induced oxidative stress and protection by vitamin E. Ann. N. Y. Acad. Sci. 669, 363–364.

Morey, M., Serras, F., Baguna, J., Hafen, E., Corominas, M., 2001. Modulation of the Ras/MAPK signalling pathway by the redox function of selenoproteins in *Drosophila melanogaster*. Dev. Biol. 238, 145–156.

Nakamura, Y., Feng, Q., Kumagai, T., Torikai, K., Ohigashi, H., Osawa, T., Noguchi, N., Niki, E., Uchida, K., 2002. Ebselen, a glutathione peroxidase mimetic seleno-organic compound, as a multifunctional antioxidant. Implication for inflammation-associated carcinogenesis. J. Biol. Chem. 277, 2687–2694.

Nishina, A., Sekiguchi, A., He, Y., Koketsu, M., Furukawa, S., 2008. Ebselen, a redox regulator containing a selenium atom, induces neurofilament M expression in cultured rat pheochromocytoma PC12 cells *via* activation of mitogen-activated protein kinase. J. Neurosci. Res. 86, 720–725.

Ramirez, R., Carracedo, J., Jimenez, R., Canela, A., Herrera, E., Aljama, P., Blasco, M.A., 2003. Massive telomere loss is an early event of DNA damage-induced apoptosis. J. Biol. Chem. 278, 836–842.

Rong, P., Bennie, A.M., Epa, W.R., Barrett, G.L., 1999. Nerve growth factor determines survival and death of PC12 cells by regulation of the bcl-x, bax, and caspase-3 genes. J. Neurochem. 72, 2294–2300.

Ryter, S.W., Kim, H.P., Hoetzel, A., Park, J.W., Nakahira, K., Wang, X., Choi, A.M., 2007. Mechanisms of cell death in oxidative stress. Antioxid. Redox Signal. 9, 49–89.

Sairanen, T., Szepesi, R., Karjalainen-Lindsberg, M.L., Karjalainen-Lindsberg, M.L., Saksi, J., Paetau, A., Lindsberg, P.J., 2009. Neuronal caspase-3 and PARP-1 correlate differentially with apoptosis and necrosis in ischemic human stroke. Acta Neuropathol.

Sekiguchi, A., Nishina, A., Kimura, H., Fukumoto, R.H., Kanoh, K., Ishihara, H., Koketsu, M., 2005. Superoxide anion-scavenging effect of 2-amino-1,3-selenazoles. Chem. Pharm. Bull. (Tokyo) 53, 1439–1442.

Sekiguchi, A., Nishina, A., Kimura, H., Fukumoto, R.H., Kogami, M., Ishihara, H., Koketsu, M., 2006. Bis-(2-amino-5-selenazoyl) ketone as a superoxide anion-scavenger. Biol. Pharm. Bull. 29, 1404–1407.

Sommen, G., Linden, A., Heimgartner, H., 2006. Selenium-containing heterocycles from isoselenocyanates: synthesis of 2-methylidene-1,3-selenazolidine derivatives. Tetrahedron 62, 3344–3354.

Takahashi, H., Nishina, A., Kimura, H., Motoki, K., Koketsu, M., Ishihara, H., 2004. Tertiary selenoamide compounds are useful superoxide radical scavengers *in vitro*. Eur. J. Pharm. Sci. 23, 207–211.

Takahashi, H., Nishina, A., Fukumoto, R.H., Kimura, H., Koketsu, M., Ishihara, H., 2005a. Selenocarbamates are effective superoxide anion scavengers *in vitro*. Eur. J. Pharm. Sci. 24, 291–295.

Takahashi, H., Nishina, A., Fukumoto, R.H., Kimura, H., Koketsu, M., Ishihara, H., 2005b. Selenoureas and thioureas are effective superoxide radical scavengers *in vitro*. Life Sci. 76, 2185–2192.

Tiano, L., Fedeli, D., Santroni, A.M., Falcioni, G., 2000. Effect of three diaryl tellurides, and an organoselenium compound in trout erythrocytes exposed to oxidative stress *in vitro*. Mutat. Res. 464, 269–277.

Vaisid, T., Kosower, N.S., Barnoy, S., 2005. Caspase-1 activity is required for neuronal differentiation of PC12 cells: cross-talk between the caspase and calpain systems. Biochim. Biophys. Acta 1743, 223–230.

Vignola, A.M., Chanez, P., Campbell, A.M., Souques, F., Lebel, B., Enander, I., Bousquet, J., 1998. Airway inflammation in mild intermittent and in persistent asthma. Am. J. Respir. Crit. Care Med. 157, 403–409.

Wang, Z., Cao, N., Nantajit, D., Fan, M., Liu, Y., Li, J.J., 2008. Mitogen-activated protein kinase phosphatase-1 represses c-Jun NH2-terminal kinase-mediated apoptosis *via* NF-kappaB regulation. J. Biol. Chem. 283, 21011–21023.

Wendel, A., Tiegs, G., 1986. A novel biologically active seleno-organic compound. VI. Protection by ebselen (PZ 51) against galactosamine/endotoxin-induced hepatitis in mice. Biochem. Pharmacol. 35, 2115–2118.

Wert, M.M., Palfrey, H.C., 2000. Divergence in the anti-apoptotic signalling pathways used by nerve growth factor and basic fibroblast growth factor (bFGF) in PC12 cells: rescue by bFGF involves protein kinase C delta. Biochem. J. 352 (Pt. 1), 175–182.

Williams, T.M., Ndifor, A.M., Near, J.T., Reams-Brown, R.R., 2000. Lead enhances NGF-induced neurite outgrowth in PC12 cells by potentiating ERK/MAPK activation. Neurotoxicology 21, 1081–1089.

Wright, J.H., Drueckes, P., Bartoe, J., Zhao, Z., Shen, S.H., Krebs, E.G., 1997. A role for the SHP-2 tyrosine phosphatase in nerve growth-induced PC12 cell differentiation. Mol. Biol. Cell 8, 1575–1585.

Zhang, M., Nomura, A., Uchida, Y., Iijima, H., Sakamoto, T., Iishii, Y., Morishima, Y., Mochizuki, M., Masuyama, K., Hirano, K., Sekizawa, K., 2002. Ebselen suppresses late airway responses and airway inflammation in guinea pigs. Free Radic. Biol. Med. 32, 454–464.

Virology Journal

BioMed Central
The Open Access Publisher

Detailed genetic analysis of hemagglutinin-neuraminidase glycoprotein gene in human parainfluenza virus type 1 isolates from patients with acute respiratory infection between 2002 and 2009 in Yamagata prefecture, Japan

Virology Journal 2011, **8**:533 doi:10.1186/1743-422X-8-533

Katsumi Mizuta (mizutak@eiken.yamagata.yamagata.jp)
Mika Saitoh (saito-mika@pref.gunma.jp)
Miho Kobayashi (kobayashi-miho@pref.gunma.jp)
Hiroyuki Tsukagoshi (tsuka-hiro@pref.gunma.jp)
Yoko Aoki (aokiyok@pref.yamagata.jp)
Tatsuya Ikeda (ikedatat@pref.yamagata.jp)
Chieko Abiko (abikoc@pref.yamagata.jp)
Noriko Katsushima (nonk@cocoa.ocn.ne.jp)
Tsutomu Itagaki (kid-tomu@hyper.ocn.ne.jp)
Masahiro Noda (nodamasa@nih.go.jp)
Kunihisa Kozawa (kozawa-ku@pref.gunma.jp)
Tadayuki Ahiko (ahikot@pref.yamagata.jp)
Hirokazu Kimura (kimhiro@nih.go.jp)

ISSN 1743-422X

Article type Research

Submission date 9 September 2011

Acceptance date 13 December 2011

Publication date 13 December 2011

Article URL http://www.virologyj.com/content/8/1/533

Virology Journal

BioMed Central
The Open Access Publisher

Detailed genetic analysis of hemagglutinin-neuraminidase glycoprotein gene in human parainfluenza virus type 1 isolates from patients with acute respiratory infection between 2002 and 2009 in Yamagata prefecture, Japan

ArticleCategory	:	Research Article
ArticleHistory	:	Received: 09-Sep-2011; Accepted: 24-Nov-2011

Katsumi Mizuta,[Aff1]
Email: mizutak@eiken.yamagata.yamagata.jp

Mika Saitoh,[Aff2]
Email: saito-mika@pref.gunma.jp

Miho Kobayashi,[Aff2]
Email: kobayashi-miho@pref.gunma.jp

Hiroyuki Tsukagoshi,[Aff2]
Email: tsuka-hiro@pref.gunma.jp

Yoko Aoki,[Aff1]
Email: aokiyok@pref.yamagata.jp

Tatsuya Ikeda,[Aff1]
Email: ikedatat@pref.yamagata.jp

Chieko Abiko,[Aff1]
Email: abikoc@pref.yamagata.jp

Noriko Katsushima,[Aff3]
Email: nonk@cocoa.ocn.ne.jp

Tsutomu Itagaki,[Aff4]
Email: kid-tomu@hyper.ocn.ne.jp

Masahiro Noda,[Aff5]
Email: nodamasa@nih.go.jp

Kunihisa Kozawa,[Aff2]

Email: kozawa-ku@pref.gunma.jp

Tadayuki Ahiko,[Aff1]
Email: ahikot@pref.yamagata.jp

Hirokazu Kimura,[Aff2 Aff6]
Corresponding Affiliation: Aff6
Phone: +81-42-5610771
Fax: +81-42-5653315
Email: kimhiro@nih.go.jp

Aff1 Yamagata Prefectural Institute of Public Health, 1-6-6 Toka-machi, Yamagata-shi, Yamagata 990-0031, Japan

Aff2 Gunma Prefectural Institute of Public Health and Environmental Sciences, 378 Kamioki-machi, Maebashi-shi, Gunma 371-0052, Japan

Aff3 Katsushima Pediatric Clinic, 4-4-12 Minamidate, Yamagata-shi, Yamagata 990-2461, Japan

Aff4 Yamanobe Pediatric Clinic, 2908-14 Yamanobe-machi, Higashimurayama-gun, Yamagata 990-0301, Japan

Aff5 Department of Virology III, National Institute of Infectious Diseases, 4-7-1 Gakuen, Musashimurayama-shi, Tokyo 208-0011, Japan

Aff6 Infectious Disease Surveillance Center, National Institute of Infectious Diseases, 4-7-1 Gakuen, Musashimurayama-shi, Tokyo 208-0011, Japan

Abstract

Background

Human parainfluenza virus type 1 (HPIV1) causes various acute respiratory infections (ARI). Hemagglutinin-neuraminidase (HN) glycoprotein of HPIV1 is a major antigen. However, the molecular epidemiology and genetic characteristics of such ARI are not exactly known. Recent studies suggested that a phylogenetic analysis tool, namely the maximum likelihood (ML) method, may be applied to estimate the evolutionary time scale of various viruses. Thus, we conducted detailed genetic analyses including homology analysis, phylogenetic analysis (using both the neighbor joining (NJ) and ML methods), and analysis of the pairwise distances of *HN* gene in HPIV1 isolated from patients with ARI in Yamagata prefecture, Japan.

Results

A few substitutions of nucleotides in the second binding site of *HN* gene were observed among the present isolates. The strains were classified into two major clusters in the phylogenetic tree by the NJ method. Another phylogenetic tree constructed by the ML method showed that the strains diversified in the late 1980s. No positively selected sites were found in the present strains. Moreover, the pairwise distance among the present isolates was relatively short.

Conclusions

The evolution of *HN* gene in the present HPIV1 isolates was relatively slow. The ML method may be a useful phylogenetic method to estimate the evolutionary time scale of HPIV and other viruses.

Keywords

Human parainfluenza virus, Maximum likelihood (ML) method, Phylogenetic analysis

Background

Human parainfluenza virus type 1 (HPIV1) of the genus *Respirovirus* and family *Paramyxoviridae* causes various acute respiratory infections (ARI) including the common cold, croup, bronchiolitis, and pneumonia [1]. Epidemiological data suggest that HPIV types 1–4 mainly infect younger children at least once, although reinfections may occur in adults [2,3]. Indeed, serological surveys indicate that at least 75% of children have been infected with HPIV1 by 5 years of age [4,5]. HPIV1 and 3 show high prevalence and are associated with up to 12% of acute lower respiratory tract infections in adults [6]. Thus, HPIVs, including HPIV1, may be major agents of ARI throughout the world [7-9].

HPIV possess two major surface glycoproteins: hemagglutinin-neuraminidase (HN) glycoprotein and fusion protein (F protein) [1]. HN glycoprotein shows multiple biological functions that include hemagglutinin and enzymatic activities as neuraminidase [3,10]. As a result, this molecule regulates viral adsorption and entry, and regulates the release of progeny virions from the infected cell surface [3]. In addition, it is suggested that HN glycoprotein is a major antigen [1]. The detailed molecular characteristics of HN glycoprotein have been confirmed in HPIV3, while those in HPIV1 remain unclear [11]. In addition, the genetic characteristics of HPIV1 are poorly understood. Thus, it is important to analyze the *HN* coding region in HPIV1.

The neighbor joining (NJ) method is frequently used in phylogenetic analysis to examine the molecular epidemiology of various viral genomes [12,13]. This method is based on a cluster classification algorithm, enabling the analysis of clusters and of the rate of viral evolution. Furthermore, the maximum likelihood (ML) method enables an estimation of the evolutionary time scale [14]. Using these methods, we conducted a detailed genetic analysis of the *HN* coding region in HPIV1 isolates from patients with ARI in Yamagata prefecture, Japan.

Methods

Patients and isolation of HPIV1

A total of 182 throat and nasal swab specimens were collected from patients attending pediatric clinics in Yamagata prefecture from May 2002 to November 2009. Informed consent was obtained from the parents of all subjects for the donation of samples used in this study. All patients were aged from 0 to 43 years (4.1 ± 5.0 years; mean ± SD). Patients were mainly

diagnosed with upper respiratory illness (URI) and wheezy bronchiolitis (Additional file 1: Table S1). URI is also known as the common cold and typically affects the upper airways, including the nose (sinusitis), throat (pharyngitis), and larynx (laryngitis) [15]. Wheezy bronchiolitis was defined as the presence of wheezing alone or chest retractions in association with URI [16].

Cell culture and virus isolation

In this study, human embryonic lung fibroblast (HEF), human laryngeal carcinoma (HEp-2), African green monkey kidney (Vero E6), Madin Darby canine kidney (MDCK), rhabdomyosarcoma (RD-18S), green monkey kidney (GMK), and human melanoma (HMV-II) cell lines were grown in Roswell Park Memorial Institute medium (Nissui No.3; Nissui Pharmaceutical Co., Ltd., Tokyo, Japan) containing 5–10% fetal bovine serum or calf serum at 37°C in a humidified atmosphere of 5% CO_2 [17]. Each cell line was prepared in 96-well tissue culture plates (Greiner Bio-One, GmbH, Frickenhausen, Germany). We inoculated the throat and nasal swabs from patients onto the plates and incubated them at 33°C in a humidified atmosphere of 5% CO_2. The cytopathic effects (CPEs) in the cells were observed 2–3 times per week. We harvested the culture supernatant when a suspected HPIV CPE was observed or a hemadsorption (HAD) test with 0.8% guinea pig erythrocytes was positive, and stored it at –80°C until analysis.

RNA extraction, RT-PCR, and sequencing

Viral RNA of HPIV1 isolates was extracted from 200 μL of the viral culture fluid by using ISOGEN (Nippon Gene, Tokyo, Japan) and was then transcribed into cDNA with M-MLV reverse transcriptase (Nippon Gene) and a random primer (Takara Bio Inc., Otsu, Japan). Reverse transcription was carried out at 30°C for 10 min, followed by incubation at 37°C for 45 min, and then incubation at 95°C for 5 min. To amplify the *HN* coding region in HPIV1 gene (nucleotide position 7245–8477, 1233 nt) by RT-PCR, we designed new primer sets using Primer Express (R) version 1.5 software (Applied Biosystems LLC, Foster City, CA) [18]. Primer sequences were as follows: first primer pair, 5′- CAG AAT TAA TCA GAC AAG AAG TRA TAT CAA G -3′ (primer HPIV-1USF, position 7165–7195), and 5′- TGA TAC GRA TTA AGA CAT TGA CAA CTT G -3′ (primer HPIV-1USR, position 8034–8061); and second primer pair, 5′- CRA GTS RAG GWA TAG RAG AYT TAG TAT TTG -3′(primer HPIV-1DSF, position 7750–7779) and 5′- GGT TRA TTT CAA CAA TRT GGA AGC AGT A -3′ (primer HPIV-1DSR, position 8529–8556). Nucleotide position was based on the sequence of *HN* glycoprotein genome in HPIV1 (Mil-48/91, GenBank accession no. U70936). Using cDNA solution, a DNA fragment of 1392 bp was amplified by PCR. Forty amplification cycles were performed at 94°C for 30 s, at 55°C for 30 s, at 72°C for 1 min, followed by a final extension at 72°C for 10 min. We analyzed the nucleotide sequences (1233b; located at 398–1633 within the *HN* gene) of the *HN* coding region. Briefly, the DNA fragment was purified with a QIAquick PCR Purification Kit (Qiagen, Valencia, CA), submitted to a cycle sequence with a Big Dye Terminator v3.1 Cycle Sequencing Kit (Applied Biosystems, Warrington, UK) using the two primer sets stated above, and purified with a spin column (AutoSeq G-50, Amersham Biosciences, Piscataway, NJ). The nucleotide sequence was determined with an automated DNA sequencer (ABI PRISM 3130 Genetic Analyzer, Applied Biosystems, Foster City, CA).

Phylogenetic analysis and calculation of pairwise distances by the NJ method

Phylogenetic analysis of the nucleotide sequence of the *HN* coding region of HPIV1 was conducted with the CLUSTAL W program available from the DNA Data Bank of Japan (http://www.ddbj.nig.ac.jp/index-j.html), and Tree Explorer version 2.12 [19].

Evolutionary distances were estimated according to Kimura's 2-parameter method, and the phylogenetic tree was constructed with the NJ method. The reliability of the tree was estimated with 1000 bootstrap replications. We used reference strains in this study to construct the phylogenetic tree. In addition, we calculated the pairwise distances for all strains, including the present isolates and reference strains to assess the frequency distribution among all HPIV1 strains and that of each intercluster of HPIV1, as previously described [20]. The GenBank accession numbers of the nucleotide sequences obtained in the present study are AB641132 to AB641313.

To evaluate the action of selective pressure on the *HN* coding regions among all HPIV1 strains, we estimated the rates of synonymous (dS) and non-synonymous (dN) changes at amino acid sites by conservative single likelihood ancestor counting (SLAC) and the fixed effects likelihood (FEL) method using ML available on the Datamonkey webserver (http://www.datamonkey.org/) [21]. The SLAC method is suitable for fast likelihood-based "counting methods" that employ either a single most likely ancestral reconstruction, weighted across all possible ancestral reconstructions, or sampling from ancestral reconstructions. The FEL method directly estimates dN and dS substitution rates at each site. These methods were performed to examine the dN and dS rates, incorporating the General Time Reversible (GTR) model of nucleotide substitution and the phylogenetic tree inferred using the NJ method. Positive ($dN > dS$) and negative ($dN < dS$) selections were predicted using these models. The *p*-value was used to classify a site as positively or negatively selected by these methods.

Phylogenetic analysis and estimation of time scale by the ML method

To construct the phylogenetic tree by the ML method, which is the best nucleotide substitution model, the GTR with gamma distributed rates across sites (GTR + Γ) [22,23] was selected by the KAKUSAN4 program version 4.0. Supplementary materials related to this program can be found online at doi:10.1111/j.1755-0998.2011.03021.x. In this study, we used three phylogenetic models of sequence evolution. One is the different rate (DR) model [14], the most general, which assumes each branch of the unrooted phylogenetic tree has a different substitution rate [24]. The DR model is used as suitable general model against which to test the assumption of constant rates of the fit of the single rate (SR) and the single rate dated tips (SRDT) models [25]. Phylogenetic analysis of ML based on the DR model was constructed with RAxML BlackBox webserver (http://phylobench.vital-it.ch/raxml-bb/index.php). All the present strains with more than 99.5% sequence similarity to any other strain were excluded from analysis. The reliability of the phylogenetic hypothesis was assessed using bootstrap analysis of 100 ML iterations. The SR model assumes the same rate of evolution in all branches (i.e., a molecular clock), and the SRDT model is an SR model that relaxes the assumption of contemporaneous sequences and uses the date of isolation of each sequence to estimate the substitution rate [24]. To estimate the rate of molecular evolution (and hence a time scale) for a phylogeny consisting of date tips,

phylogenetic analyses by ML based on the SR and SRDT models were performed using the TipDate webserver (http://mobyle.pasteur.fr/cgi-bin/portal.py?#forms::tipdate) [24]. The likelihood of the SR and SRDT models (with likelihood L_0) were compared to that of the DR model (with likelihood L_1) in a likelihood ratio test (LRT) [14] of the fit of the model. The test statistic is the difference in the log likelihood (Δ) between the SR or SRDT model and the DR model. In the LRT statistic, twice the ratio of log likelihoods (L_1/L_0) ($2\Delta^*$) is expected to be χ^2 distributed with degrees of freedom equal to their models. The DR model has $2n$-3 free parameters, the SR model has n-1, and the SRDT model has n-2 (a tree of n tips). In the LRT of the fit of the SR and SRDT models compared with the DR, if the SR model is rejected in favor of the DR model but the SRDT model is not, the SRDT model can be accepted as no worse a description of the evolution date than the DR model. A P value of ≥ 0.05 was considered statistically significant for the phylogenetic models. The resulting phylogenetic trees were described using TreeExplorer version 2.12. The rates of nucleotide substitution, the date estimating the root of the tree and the corresponding upper and lower 95% confidence intervals (CIs) were calculated under the SRDT model using the TipDate webserver.

Results

Phylogenetic analysis of the nucleotide sequences of the *HN* coding region in HPIV1 by the NJ method

The partial nucleotide sequences (1233 nt) of *HN* glycoprotein gene in a total of 182 isolates and 3 reference strains were analyzed. The phylogenetic tree based on the nucleotide sequences by the NJ method is shown in Figure 1. The enlarged cluster shows the HPIV1 strains. The phylogenetic tree containing the isolated and reference strains was classified into two unique clusters with the exception of three Yamagata strains (HPIVi/Yamagata/2002/1433, HPIVi/Yamagata/2002/1565, and HPIVi/Yamagata/2003/1122), clusters 1 and 2, and these strains were classified into different clusters from the reference strains. The number of detected strains in each cluster on the phylogenetic tree was as follows: cluster 1, 84 strains including strains isolated during 2004–2009; and cluster 2, 95 strains from 2003 to 2005, and 2007 to 2009.

Figure 1 Phylogenetic tree of HN region by NJ method. Phylogenetic tree based on the nucleotide sequence of the *HN* coding region (1233nt), including the present strains (182) and representative reference strains (3). HPIV3 was used as an outgroup. Distance was calculated according to Kimura's 2-parameter method, and the tree was plotted with the neighbor-joining method. Reference strains are shown in italic type. The larger tree was simply expanded for HPIV1 strains, to clarify the distance of each of the minor clusters in the trees. The tree was constructed by neighbor-joining analysis with labeling of the branches showing at least 70% bootstrap support. The representation of the strain was changed from Yamagata/20XX/ZZZZ to YXX/ZZZZ

Likelihood ratio test (LRT) of the fit of the models and timescale evolution of the *HN* coding region in HPIV1 by the ML method

Based on the SRDT model [24,26], we constructed another phylogenetic tree consisting of dated tips by using the nucleotide sequences of the HPIV1 *HN* coding region of 43 isolated strains from patients in Yamagata prefecture and 3 reference strains by using the ML method. As a result, the SR model was rejected as an adequate description of the evolution of the HPIV1 *HN* coding region ($p < 0.05$). Therefore, the SRDT model was not significantly worse than the DR model, indicating that this model adequately describes the substitution process ($p = 0.06$). Through these processes, we obtained a phylogenetic tree by the ML method. The year of the first major division in the present tree was estimated at 1950 (Figure 2; 95% CIs of 1935 to 1955). In addition, the ancestral strains of the present strains subdivided around 1987. Further division occurred around 1989, resulting in the formation of two major clusters (clusters 1 and 2). Furthermore, we estimated the rate of molecular evolution from the tree as 7.68×10^{-4} substitutions per site per year (95% CIs of 4.80×10^{-4} to 1.07×10^{-3}).

Figure 2 Phylogenetic tree of HN region by ML method. Phylogenetic tree based on the nucleotide sequence of the *HN* coding region (1233 nt), including the present strains (43) and representative reference strains (3), with branch lengths scaled under the SRDT model. Reference strains are shown in italic type

Analysis of pairwise distances, substitutions of the second binding site, and selective pressure of the *HN* coding region in HPIV1

The nucleotide and amino acid sequence identities among all 182 isolates were high at 92.6–100% and 96.0–100%, respectively. In addition, we calculated the intercluster distances of HPIV1 from the distribution of the pairwise distances. Based on the nucleotide sequences, the pairwise distance was 0.018 ± 0.013 [mean ± SD, Figure 3a] for the 182 present and 3 reference strains. The pairwise intercluster distances were as follows: cluster 1, 0.003 ± 0.002 (Figure 3b); and cluster 2, 0.008 ± 0.005 (Figure 3c). Cluster 2 showed a large pairwise intercluster distance, whereas that for cluster 1 was small. However, irregular peaks of pairwise distance are seen in Figure 3, and we were not able to genotyping the present strains based on the pairwise distance value. Next, amino acid substitutions in the analyzed *HN* coding region in the present strains were found at 31sites (detailed substitution data not shown). Among these was an essential substitution of the second binding site, N523S. This substitution (N523S) was seen in seven of the present strains (HPIVi/Yamagata/2007/1577, HPIVi/Yamagata/2007/1599, HPIVi/Yamagata/2007/2211, HPIVi/Yamagata/2007/2072, HPIVi/Yamagata/2007/2354, HPIVi/Yamagata/2007/2274, and HPIVi/Yamagata/2008/413). These strains belonged in cluster 2 (Figure 1).

Figure 3 Distributions of pairwise distances for HPIV1 of HN region. (a) Distribution of pairwise distances for the 182 present and 3 reference strains. (b) Distribution of pairwise intercluster distances for cluster 1. (c) Distribution of pairwise intercluster distances for cluster 2

Selection pressure analysis was performed in the present strains, and the results showed a low mean dN/dS ratio (0.17) (95% likelihood profile-based CIs, CI = 0.13–0.23) by the SLAC method. Thus, the nucleotide substitutions predicted were largely synonymous. The dN/dS ratios of the individual sites in the *HN* coding region were calculated by the SLAC and FEL methods significant at the $p < 0.1$ level. However, neither method detected a positively selected site.

Discussion

In this study, we performed a detailed genetic analysis of *HN* glycoprotein gene in HPIV1 isolates from patients with ARI during 2002–2009 in Yamagata prefecture, Japan. The phylogenetic tree constructed by the NJ method showed that the present HPIV1 isolates were divisible into two major genetic clusters (Figure 1). The other tree constructed by the ML method showed that the year of the first major division was estimated at 1950, and the ancestral strains further subdivided at around 1987, resulting in three clusters (one minor and two major, Figure 2). The strains belonging to the two major clusters subdivided into many clusters after 2000. The present HPIV1 isolates showed an overall high level of nucleotide sequence identity (92.6–100%) of the *HN* coding region. Pairwise distance values based on the nucleotide sequences among the present strains were relatively low (less than 0.06). In addition, there were no positively selected sites found. These results suggest that several lineages of highly conserved *HN* gene in HPIV1 were prevalent in Yamagata prefecture. The present strains could not be provisionally type assigned from the pairwise distance values. Thus, the accumulation of large amounts of data may be needed to genotype HPIV1 based on pairwise distance.

Homology and phylogenetic analysis by the NJ method is frequently used in molecular epidemiological studies of various viruses. Homology analysis based on nucleotide sequences mainly shows the similarities of the analyzed genes among the strains. Phylogenetic analysis by the NJ method can give an estimation of the viral evolution rate and cluster classification. Furthermore, the ML method can enable analysis of the time scale of the evolution of viral genes. In the present study, we were able to estimate the viral evolution rate of HPIV1, cluster classification, and the evolutionary time scale of the present isolates by applying the NJ and ML methods to the detailed phylogenetic analysis of the *HN* coding region in HPIV1. There is currently little information available regarding the molecular evolution of the *HN* coding region in HPIV (HPIV1 to 4). Furthermore, the rate of molecular evolution is very low (7.68×10^{-4} substitutions/site/year) in the present strains. Previous reports suggest that the rate of another gene of respiratory viruses belonging to *Paramyxoviridae,* such as respiratory syncytial (RS) virus, is higher (1.8×10^{-3} substitutions/site/year) than that of the present data [27]. The reason for the difference is unknown at present. However, it is possible that genome properties other than size, such as polarity or structure, may be associated with substitutions of the viral genome [27]. Further studies on the detailed mechanisms of viral genome substitution may be needed. Additional sequence data and further structural analysis are required to demonstrate the mechanisms of the molecular evolution of HPIV1.

HPIV is classified into four serotypes (HPIV1 to 4), all of which can cause various ARI in humans, such as URI, croup, bronchitis, and pneumonia [1]. Previous reports suggest that HPIV1 and 3 are the dominant viruses in children with ARI [28]. In addition, HPIV is a major causative agent of virus-induced asthma [29]. Thus, HPIV1 is a major agent of ARI, along with other viruses, such as adenovirus, RS virus, human metapneumovirus, and rhinovirus [30]. However, the molecular epidemiology of HPIVs is poorly understood, and only a few reports on the molecular epidemiology of HPIV1 are available. For example, Henrickson and Savatski analyzed the longitudinal evolution of the *HN* coding region in 13 strains of HPIV1 isolated in the United States [31]. The results showed that the antigenic and genetic subgroups are very stable. Another report suggested that two distinct genotypes of HPIV were detected during the

1991 Milwaukee epidemic [32]. In the present study, we used HPIV1 isolates from patients with ARI and studied the evolution of HN protein, based on phylogenetic analyses using both the ML and NJ methods and the rate of the substitutions of nucleotides. The results showed that HN protein is highly conserved. In addition, no positively selected sites were detected. To our best knowledge, this is the first report of these findings in HPIV1.

The distribution of amino acids affects the structure of the *HN* coding region in HPIV1, and previous reports show that substitutions of amino acids in HN glycoprotein reveal second receptor binding sites [33,34]. For example, substitutions at Asn173 and Asn523 are critical for the formation of a second binding site. In particular, these substitutions affect, for example, the inhibitor in hemagglutination inhibition (HI) assays and infection of culture cells. However, the second receptor binding site did not significantly affect the growth or fusion activity of HPIV1. Substitutions at N523S were found in seven of the present strains, but there were no substitutions at Asn173. Thus, we thought that N523S may not be significantly associated with infectivity or pathogenicity.

Furthermore, we then examined selective pressure by counting and the ML method. Analysis of selection pressure in the present strains showed that dS substitutions predominated over dN substitutions, and no positively selected sites (substitution) were found in HN protein in the present HPIV1 strains. The evolution of the present strains may be largely driven by purifying selection. Compared with HPIV3, little is known about the detailed biological properties of HN glycoprotein in HPIV1. As an essential molecule of these viruses, further analysis of the biological properties of HN glycoprotein in HPIV1 is required [35].

Although detailed data of the antigenic and catalytic sites of HN molecules in HPIV3 is relatively clear [36], such information regarding HPIV1 is not yet known. Moreover, the epidemiology and molecular epidemiology of HPIV is not exactly known. Thus, further and larger epidemiological/molecular epidemiological studies are required to give better understanding of the etiology of HPIVs, including HPIV1.

Conclusions

Our study suggested that several prevalent lineages of *HN* gene are highly conserved and evolution occurred from the late 1980s in HPIV1 in Yamagata prefecture. Viral evolution was estimated by detailed phylogenetic analyses using the NJ and ML methods. These methods offer a new understanding of the genetic evolution of *HN* gene.

Abbreviations

HPIV1: Human parainfluenza virus type 1, ARI: Acute respiratory infections, HN: Hemagglutinin-neuraminidase, NJ: Neighbor joining, ML: Maximum likelihood, URI: Upper respiratory illness, CPE: Cytopathic effect, HAD: Hemadsorption, dS: Synonymous, dN: Non-synonymous, SLAC: Single likelihood ancestor counting, FEL: Fixed effects likelihood, GTR: General time reversible, DR: Different rate, SR: Single rate, SRDT: Single rate dated tips, LRT:

Likelihood ratio test, CI: Confidence interval, RS: Respiratory syncytial, HI: Hemagglutination inhibition

Competing interests

The authors declare that they have no competing interests.

Authors' contributions

KM and HK designed the research project; MS, MK, HT, YA, TI, CA, and NK performed the research; TI, MN, KK, and TA contributed the analytical tools; KM, MS, MK, and HK analyzed the data, and KM, MS, and HK wrote the paper. All authors read and approved the final manuscript.

Acknowledgements

This work was partly supported by a Grant-in-Aid from the Japan Society for the Promotion of Science and for Research on Emerging and Re-emerging Infectious Diseases from the Ministry of Health, Labour and Welfare, Japan.

References

1. Karron RA, Collins PL: **Parainfluenza viruses.** In *Fields virology. volume 1.* 5th edition. Edited by Knipe DM, Howley PM. Philadelphia: Lippincott Williams & Wilkins; 2007:1497–1526.

2. Griffin MR, Walker FJ, Iwane MK, Weinberg GA, Staat MA, Erdman DD, New Vaccine Surveillance Network Study Group: **Epidemiology of respiratory infections in young children: insights from the new vaccine surveillance network.** *Pediatr Infect Dis J* 2004, **23** (11 Suppl.):S188–192.

3. Moscona A: **Entry of parainfluenza virus into cells as a target for interrupting childhood respiratory disease.** *J Clin Invest* 2005, **115**:1688–1698.

4. Parrott RH, Vargosko A, Luckey A, Kim HW, Cumming C, Chanock R: **Clinical features of infection with hemadsorption viruses.** *N Engl J Med* 1959, **260**:731–738.

5. Parrott RH, Vargosko AJ, Kim HW, Bell JA, Chanock RM: **Acute respiratory diseases of viral etiology. III. parainfluenza. Myxoviruses.** *Am J Public Health Nations Health* 1962, **52**:907–917.

6. Matsuse H, Kondo Y, Saeki S, Nakata H, Fukushima C, Mizuta Y, Kohno S: **Naturally occurring parainfluenza virus 3 infection in adults induces mild exacerbation of asthma**